Numerical simulation of the Benjamin-Feir instability and its consequences

Dmitry Chalikov[a)]
Earth System Science Interdisciplinary Center (ESSIC), University of Maryland, Room 2207, 224 CSS Building, College Park, Maryland 20742-2465

(Received 29 October 2005; accepted 20 October 2006; published online 25 January 2007)

Full nonlinear equations for one-dimensional potential surface waves were used for investigation of the evolution of an initially homogeneous train of exact Stokes waves with steepness $AK=0.01-0.42$. The numerical algorithm for the integration of nonstationary equations and the calculation of exact Stokes waves is described. Since the instability of the exact Stokes waves develops slowly, a random small-amplitude noise was introduced in initial conditions. The development of instability occurs in two stages: in the first stage the growth rate of disturbances was close to that established for small steepness by Benjamin and Feir [J. Fluid. Mech. **27**, 417 (1967)] and for medium steepness [McLean, J. Fluid Mech. **114**, 315 (1982)]. For any steepness, the Stokes waves disintegrate and create random superposition of waves. For $AK<0.13$, waves do not show a tendency to breaking, which is recognized by approaching a surface to non-single-value shape. Sooner or later, if $AK>0.13$, one of the waves increases its height, and finally it comes to the breaking point. For large steepness of $AK>0.35$ the rate of growth is slower than for medium steepness. The data for spectral composition of disturbances and their frequencies are given. © *2007 American Institute of Physics*. [DOI: 10.1063/1.2432303]

I. INTRODUCTION

This work should be considered as further development of Stokes wave instability theory.[1,2] It also represents a preliminary study intended for development of two-dimensional interactive simulation of surface waves and the air boundary layer above waves. Until recently, the investigations of the interaction between wind and waves were performed mainly for a single periodic wave surface assigned by a linear theory even for the cases when the amplitude of the wave was not small. Such investigations based on Reynolds equations for a boundary layer were started in Refs. 3 and 4. Chalikov's model was used later for investigation of different problems of wave boundary layer (WBL) (see, for example, Refs. 5–8). A more advanced model of WBL was recently developed in Ref. 9. The problem with all these models is that the monochromatic waves represent an idealized situation that is rarely observed in natural conditions. A generalization of the monochromatic results (obtained for the stationary flow) for the multimode wave field is routinely based on a linear assumption. Applicability of this assumption for finite amplitude waves is doubtful. Besides, the waves assigned by linear theory do not describe the typical shape of dominant waves, which usually have sharp crests and gentle troughs. It was established in technical fluid mechanics that even small modifications of patterns change the form drag significantly. Evidently, sharp-crested waves create a form drag much larger than do smooth waves with the same height. Additionally, surface unsteadiness supports the strong nonsteadiness of both flow and pressure fields. This is presented correctly in perturbation theory only for very small amplitudes. It became evident several years ago[10] that a more realistic presentation of nonstationary wave surface is needed. The best way is evidently a construction of a coupled wind-wave model, based on the nonstationary equations for air and water. Their solutions are matched through moving interface. The first such interactive numerical experiments have been described in Ref. 11. This approach became possible after the development of numerical modeling for surface gravity waves. It was intended at the initial stage of this work using the numerical approach developed by Dold and Peregrine[12] (hereafter D-P) and described in detail in Ref. 13. Actually, D-P was a first model for realistic simulation of the surface waves based on the principal potential equations, contrary to numerous approaches that used the simplified equations or the perturbation theory (see references in Ref. 14 and more information in Ref. 15). Recently, the D-P model was applied to investigation of the evolution of an initially uniform wave train.[16] It was observed that wave energy becomes concentrated in a group of steep waves which can break if initial wave energy is large enough. While studying the D-P approach, we found that a simpler and more precise method can be constructed on a basis of conformal mapping. The numerical scheme in this method is based on the Fourier-transform method, so the approximations of all derivatives and nonlinear terms are much more precise than in any scheme based on local approximation. Contrary to the D-P scheme, our scheme does not need the smoothing in physical space, just routine high wave number dumping in Fourier space. For the stationary problem, this mapping represents the classical complex variable method (e.g., Refs. 17 and 18) originally developed by Stokes.[19,20] In a stationary problem, this method employs the velocity potential Φ and the stream function Ψ as the independent variables. Actually, an approach based on a nonstationary conformal mapping was formulated earlier several times. It was introduced in Ref. 21 and then considered in Refs. 22–24. In Refs. 25 and 26, this approach was used for investigating the Rayleigh-Taylor in-

stability and the generation of surface singularities. A new way of deriving equations and a description of a numerical scheme (and its validation), as well as the results of long-term simulations, were described in detail in Ref. 27 (hereafter ChSh). The ChSh numerical approach is based on nonstationary conformal mapping for finite depth. This allows rewriting of the principal equations of potential flow with a free surface in a surface-following coordinate system. The Laplace equation retains its form, *and* the boundaries of the flow domain (i.e., the free surface and, in the case of finite depth, the bottom) are coordinate surfaces in the new coordinate system. Accordingly, the velocity potential in the entire domain receives a standard representation based on its Fourier expansion on the free surface. As a result, the hydrodynamical system (without any simplifications) is represented by two simple evolutionary equations that can be solved numerically in a straightforward way. The advantages of this approach were briefly discussed in Ref. 28; later, in Ref. 29, the method developed was used to demonstrate the nonlinear properties of steep waves. In principle, the ChSh method is similar to the method developed by Meiron *et al.*[24] However, they concluded that this method is applicable only to "moderately distorted geometry." In Ref. 29, it was also noticed that conformal mapping above a curvilinear boundary can result in a strongly nonuniform grid. This conclusion makes sense for schemes with low resolution only: for an approximation of the Stokes wave profile, only $N=64$ points were used in the cited paper. In such a presentation, the Stokes wave is approximated inaccurately, and this resolution is too poor for numerical integration in time. In our work, this problem does not arise because we exploited thousands of points. Zakharov *et al.* used even up to 10^6 Fourier modes.[39] Above the smooth parts of the surface this resolution can be excessive, but it is sufficient above patterns with large curvature. The accuracy of the scheme is controlled with integral invariants of the problem. All these technical problems were resolved in the early stage of constructing the ChSh model.[27]

Recently, the ChSh model was applied to the simulation of the wave's evolution with different initial conditions.[30] Numerical experiments with initially monochromatic waves with different steepness showed that the model was able to simulate breaking conditions when the wave obtained a strong asymmetry and surface finally becomes a multivalued function of the horizontal coordinate. An estimate of the critical initial wave height that divides between nonbreaking and eventually breaking waves is obtained. Simulations of nonlinear evolution of a wave field were represented initially by two modes with close wave numbers (amplitude modulation) and a wave field with a phase modulation. Both runs result in the appearance of large and very steep waves; these also break if the initial amplitudes are sufficiently large. The breaking process develops very quickly, so the period of multivalued surface existence is very short. Formally, instability exhibits itself in the fast growth of high wave number modes, but physically, a tendency for splitting of falling volume is quickly developing, which makes it impossible to apply conformal mapping, potential approximation, and generally, equations of fluid mechanics for single phase of fluid.

Next, the model was applied to simulation of the nonbreaking evolution of wave fields with a large number of modes for many periods of dominant waves.[14] The statistical characteristics of nonlinear wave fields for waves of different steepness were investigated: spectra, kurtosis and skewness, dispersion relation, and lifetime. The prime result that a wave field may be presented as a superposition of linear waves is valid only for small amplitudes. It was shown as well that nonlinear wave fields are rather a superposition of Stokes waves, not linear waves.

In this paper, the investigation of nonlinear properties of one-dimensional (1-D) surface wave is done for the wave train of Stokes waves. The stability of such an initially uniform wave train was a subject of many investigations. It was shown that for weakly nonlinear waves, it is unstable to low-frequency perturbations,[31] Benjamin and Feir[1] (hereafter B-F). Numerical investigations[32] extended these results to large-amplitude waves and long-wave perturbations. The most detailed results were obtained in Ref. 2, where investigated numerically the stability of exact Stokes waves to two-dimensional (2-D) small-amplitude disturbances. The evolution of disturbances was investigated with linearized equations. The experimental investigation of the 2-D instability of finite-amplitude waves was performed in Ref. 33.

This work deals with 1-D finite-amplitude Stokes waves, disturbed by small-amplitude initial noise on a basis of fully nonlinear equations. In this case, the development of disturbances and their interaction with initial waves are simulated in a fully nonlinear manner, regulated by conservations of total energy and momentum.

II. THE GOVERNING EQUATIONS

Consider the periodic one-dimensional deep-water waves, which dynamics is described by principal potential waves equations. Due to the periodicity condition, the conformal mapping for infinite depth can be represented by the Fourier series (see details in ChSh):

$$x(\xi,\zeta) = \xi + x_0(\tau) + \sum_{-M\leqslant k<M, k\neq 0} \eta_{-k}(\tau)\exp(k\zeta)\,\vartheta_k(\xi), \tag{2.1}$$

$$z(\xi,\zeta) = \zeta + \eta_0(\tau) + \sum_{-M\leqslant k<M, k\neq 0} \eta_k(\tau)\exp(k\zeta)\,\vartheta_k(\xi), \tag{2.2}$$

where x and z are Cartesian coordinates, ξ and ζ are conformal surface-following coordinates, τ is a time, and η_k are the coefficients of Fourier expansion of the free surface $\eta(\xi,\tau)$ with respect to the new horizontal coordinate ξ:

$$\eta(\xi,\tau) = h[x(\xi,\zeta=0,\tau), t=\tau] = \sum_{-M\leqslant k\leqslant M} \eta_k(\tau)\,\vartheta_k(\xi), \tag{2.3}$$

ϑ_k denotes the functions

$$\vartheta_k(\xi) = \begin{cases} \cos k\xi, & k \geqslant 0, \\ \sin k\xi, & k < 0; \end{cases} \tag{2.4}$$

M is the truncation number; $x_0(\tau)$ can be chosen arbitrarily, though it is convenient to assume that $x_0(\tau)=0$.

Nontraditional presentation of the Fourier transform with definition (2.4) is, in fact, more convenient for calculations because $(\vartheta_k)_\xi = k\vartheta_{-k}$ and $\Sigma(A_k\vartheta_k)_\xi = -\Sigma kA_{-k}\vartheta_k$. Thus, the Fourier coefficients A_k form the real array $A(-M:M)$, thus making possible a compact programming in FORTRAN90.

Note that the definitions of both coordinates ξ and ζ are based on Fourier coefficients for surface elevation. It follows then from Eqs. (2.1) and (2.2), that the time derivatives z_τ and x_τ for Fourier components are connected by the simple relation

$$(x_\tau)_k = (z_\tau)_{-k}. \tag{2.5}$$

Due to conformity, the Laplace equation retains its form in (ξ,ζ) coordinates. It is shown by ChSh that potential waves equations can be represented in the new coordinates as follows:

$$\Phi_{\xi\xi} + \Phi_{\zeta\zeta} = 0, \tag{2.6}$$

$$z_\tau = x_\xi g + z_\xi f, \tag{2.7}$$

$$\Phi_\tau = f\Phi_\xi - \frac{1}{2}J^{-1}(\Phi_\xi^2 - \Phi_\zeta^2) - z, \tag{2.8}$$

where (2.7) and (2.8) are written for the surface $\zeta=0$ (so that $z=\eta$, as represented by expansion (2.1); J is the Jacobian of the transformation

$$J = x_\xi^2 + z_\xi^2 = x_\zeta^2 + z_\zeta^2, \tag{2.9}$$

g is an auxiliary function

$$g = (J^{-1}\Phi_\zeta)_{\zeta=0}, \tag{2.10}$$

and f is a generalization of the Hilbert transform of g, which, for $k\neq 0$, may be defined in Fourier space as

$$f_k = g_{-k}, \quad g_k = -f_{-k}, \tag{2.11}$$

following in fact from Eq. (2.5).

Equations (2.6)–(2.8) are written in the nondimensional form with the following scales: length L, where $2\pi L$ is the (dimensional) period in the horizontal, time $L^{1/2}G^{-1/2}$, and the velocity potential $L^{3/2}G^{-1/2}$ (G is the acceleration of gravity). Capillarity and external pressure were not taken into account in this investigation.

The boundary condition assumes the vanishing of vertical velocity

$$\Phi_\zeta(\xi, \zeta \to -\infty, \tau) = 0. \tag{2.12}$$

The solution to the Laplace equation (2.6) with boundary condition (2.12) readily yields to Fourier expansion, which reduces the system (2.6)–(2.8) to a 1-D problem:

$$\Phi = \sum_{-M\leqslant k\leqslant M} \phi_k(\tau)\exp(k\zeta)\vartheta_k(\xi), \tag{2.13}$$

where ϕ_k are Fourier coefficients of the surface potential $\Phi(\xi,\zeta=0,\tau)$. Equations (2.6)–(2.8), (2.10), and (2.11) constitute a closed system of prognostic equations for the surface functions $z(\xi,\zeta=0,\tau)=\eta(\xi,\tau)$ and $\Phi(\xi,\zeta=0,\tau)$.

For time integration, the fourth-order Runge-Kutta scheme was used. The choice of time step was done empirically. For example, for $M=100$, a time step was equal to 0.01. For $M=1000$, it was 0.002. Increasing the local steepness and surface curvature often forces application of smaller time steps. The scheme is so simple that a core of a FORTRAN95 program fits in 15 lines.

A specific problem is that initial data are normally given in the Cartesian coordinates. These need to be converted to the (ξ,ζ) coordinates. For this purpose, and for postprocessing of the results, an interpolating algorithm based on the periodic high-order spline functions has been developed. The algorithm carries out the transformation with high accuracy.

The problem of validation of numerical scheme was discussed by ChSh in Refs. 14 and 27. The scheme turned out to be very precise. This is not surprising, because, contrary to the initial form of the equations, the equations written in conformal coordinates become simple one-dimensional evolutionary equations, which can be solved accurately with the Fourier transform method without the use of any local approximation. Remarkably, conformal mapping made possible a reproduction of the essential stages of the breaking process when the surface ceases to be a single-valued function.[27] This initial stage of wave breaking exhibits a sharp jet originating from a wave crest. The integration in this case is always terminated; but due to the high accuracy of the scheme, however, the numerical and physical instabilities follow each other very closely.

III. INITIAL CONDITIONS: CALCULATING THE EXACT STOKES WAVES

Following Ref. 2, the initial conditions for the nonstationary problem were assigned as a superposition of exact Stokes waves and small-amplitude noise. For the case of infinite depth (Stokes waves), a method based on expansion of the Fourier coefficients of the surface height in the power series of the wave amplitude was originally proposed by Stokes,[19,20] who in his latter work obtained a fifth-order approximation. In recent studies, the method has been further developed into a recursive scheme which produces consecutive power expansion coefficients. Solutions for Stokes waves have been obtained in Refs. 34, 32, and 36. An algorithm[35] was used in the investigation of stability of finite-wave amplitudes in Ref. 32. In Ref. 37, the calculations were carried out up to 170 terms. A full set of simple and very fast numerical methods of obtaining the exact stationary solution for gravity and gravity-capillary waves for deep water was developed in Ref. 27 and for shallow water in Ref. 38. In this paper, only the algorithm for stationary gravity waves in deep water (Stokes waves) will be described.

For the stationary problem, the method of conformal mapping is a well-known approach based on using the velocity potential Φ and the stream function Ψ as the independent variables (e.g., Ref. 18). It is easy to show that in this case,

$$\Phi = -c\xi + \Phi_0, \quad \Psi = c\zeta + \Psi_0, \tag{3.1}$$

where $-c$ is the velocity of the mean flow, $\Phi_x = -\Psi_z$ and $\Phi_z = \Psi_x$ are the horizontal and the vertical Cartesian velocity components, respectively, and Φ_0, Ψ_0 are constants. For the stationary version of system (2.6)–(2.8), to describe progressive waves, the periodicity condition on Φ, which implies a zero mean flow velocity, must be replaced by the weaker condition of periodicity of the velocity components; i.e., of the spatial derivatives of Φ. In a coordinate system moving with the wave's phase velocity c, the mean flow velocity is equal to $-c$, and the velocity potential Φ is given by relations (3.1), where Φ_0 must be allowed to depend on time (since a steadiness is assumed for the velocity field rather than the velocity potential). Consequently, with the external pressure $p=0$, system (2.6)–(2.8) is strictly reduced to one equation written for the surface $\zeta=0$:

$$\tfrac{1}{2}c^2 J^{-1} + z = a, \tag{3.2}$$

where $a = d\Phi_0/d\tau$, and since the left-hand side of 3.2 does not depend on time, a is a constant (so that the dependence Φ_0 on τ may only be linear). Equation (3.2) looks deceptively simple, but its numerical solution is tricky. The solutions in the form of Fourier expansion coefficients for the surface height were sought with an iterative algorithm. The conformal mapping with surface boundary condition (3.2) is determined by the coefficients η_k through the relationships (2.1) and (2.2). With $\varsigma=0$, Eqs. (2.1) and (2.2) may serve as a parametric representation of the surface. Equation (3.2) can be rewritten in the form

$$\log\left(\frac{1}{2}c^2\right) - \log J = \log(a - z). \tag{3.3}$$

Introducing the complex variables $\rho = \xi + i\zeta$ and $r(\rho) = x(\xi,\zeta) + iz(\xi,\zeta)$, and denoting $w = d(\log\tau)/d\rho$, it can be seen that

$$\log J = 2\,\mathrm{Re}(w), \quad z_\xi = \mathrm{Im}[\exp(w)]. \tag{3.4}$$

Thus, if the Fourier expansion for $\log J$ is known, $\mathrm{Im}(w)$ can be found via the Hilbert transform as in the second equation of (2.11), after which w and $\exp(w)$ can be calculated at the grid points. This yields z_ξ, and after finding the corresponding Fourier coefficients by direct Fourier transform, z can be obtained by integration in Fourier space. Thus, z can be easily found if $\log J$ is known. This allows reducing the differential relationship (3.3) to an equation with an integral operator, which may be solved by a simple iterative procedure.

Assuming that z is an even function of ξ, it is convenient to choose

$$s = \tfrac{1}{4}(\log J_{\xi=0,\zeta=0} - \log J_{\xi=\pi,\zeta=0}) \tag{3.5}$$

as the parameter determining the amplitude of the wave (in linear approximation, s is equal to amplitude). With χ^n denoting the value of any variable χ on nth iteration, the scheme can be written as follows:

(a) Assume $n=0$, $\log J^0 = 2s\exp\zeta\cos\xi$ (this is a solution of the linearized problem).

(b) For given $\log J^n$, use the Hilbert transform (2.11), complex exponent calculation, and integration in Fourier space to find z^n, as described above. If condition $\max|z^n - z^{n-1}| < \varepsilon$ is met (ε is prescribed accuracy), the z^n is a solution within the accuracy given.

(c) Let

$$a = a^{n+1} = [\exp(4s)z^n(\zeta=0) - z^n(\zeta=\pi)] \times [\exp(4s) - 1]^{-1}. \tag{3.6}$$

This will ensure relation (3.5) for the next iteration. Grid values for $\log J^{n+1}$ are calculated with

$$\log J^{n+1} = -\log(a^{n+1} - z^n) + [\log(a^{n+1} - z^n)]_0. \tag{3.7}$$

(d) Find the Fourier expansion of $\log J^{n+1}$, let $n = n+1$ and return to step (b).

The last term in (3.7) allows us to find the phase velocity on the $(n+1)$th step: in accordance with (3.3); this term is equal to $\log\left[\frac{1}{2}(c^{n+1})^2\right]$. Equality (3.7) is based on the fact that the mean value of $\log J$ over ξ is zero, which follows from the first equation of relation (3.4), as $w \to 0$ when $\zeta \to -\infty$.

Figure 1 illustrates some results of the calculations of Stokes waves for number of modes $M=3200$, and $\varepsilon = 10^{-11}$. The algorithm described above converges up to steepness $AK=0.44$. Stokes wave with $AK=0.44$ is unstable, and being accepted as the initial condition for nonstationary problem disintegrates very quickly. Stokes wave with $AK=0.43$ reveals the periodic regime (see Fig. 1 in Chalikov[14]), which

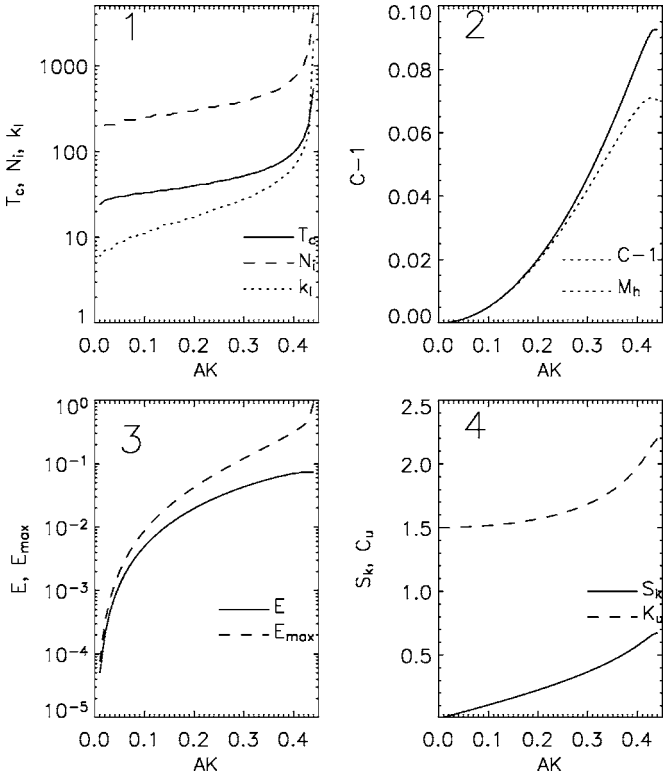

FIG. 1. Characteristics of stationary solutions for Stokes waves as functions of steepness $AK=(0.01-0.44)$: (1) T_c—time of calculation in milliseconds, N_i—number of iterations, k_l—number of Fourier mode with amplitude less than 10^{-11}; (2) $C-1$ (C—a phase velocity, M_h—horizontal momentum; (3) $E=E_p+E_k$—total energy, where E_p—potential energy, E_k—kinetic energy; (4) skewness Sk, kurtosis Ku.

can exist for at least hundreds of periods. For $AK<0.427$, the Stokes wave is conditionally stable in absence of disturbances. For steeper Stokes waves ($AK>0.43$), the crest instability develops.[32] The disturbances with amplitudes less than ε can grow, and finally the Stokes wave disintegrates. A further increasing of the accuracy results in a longer life expectancy for the Stokes wave.

The calculation of the most steep Stokes wave with $AK=0.44$ and number of modes $M=3200$ was done on a Dell PC (speed 3.11 GHz) with 550 iterations performed for 4.17 s. The number of modes with amplitudes larger than ε equals 1932 in this case (Fig. 1, panel 1). Calculations for $AK=0.30$ took 52 iterations and 0.037 s. In this case the number of modes needed was 28. Phase speed (panel 2) reaches the maximum value ($c=1.0926$) at $AK=0.44$. Total horizontal momentum M_h, and potential E_p and kinetic E_k energies of waves were calculated with exact relations

$$M_h=(2\pi)^{-1}\int_0^{2\pi}\Phi z_\xi d\xi,\quad E_p=(2\pi)^{-1}\int_0^{2\pi}z^2x_\xi d\xi,$$
$$E_k=(2\pi)^{-1}\int_0^{2\pi}\Phi\Phi_\zeta d\xi. \tag{3.8}$$

Dependence of M_h and excess of phase velocity above linear value $C-1$ on steepness AK is shown in Fig. 1, panel 2. It is interesting that values of M_h and $C-1$ coincide with high accuracy for small steepness. Dependence of the sum of kinetic and potential energies, i.e., $E=E_p+E_k$, on AK is shown in panel 3 (Fig. 1, solid line). Naturally, the energy is growing with steepness, but not proportionally to $(AK)^2$ because of the increasing of the sharpness of crest and the vertical asymmetry of surface (see dependence of the skewness Sk and kurtosis Ku for Stokes waves on steepness AK in panel 4, Fig. 1). The examples of profiles of Stokes waves are shown in Fig. 2 together with profiles of columnar potential e_p and kinetic e_k energies, calculated by relations

$$e_p=\frac{z^2}{2},\quad e_k=\int_{-H}^{z}(u^2+w^2)dz, \tag{3.9}$$

where u and w are the velocity components calculated through the two-dimensional velocity potential φ. The integral in (3.9) was calculated in a stretched vertical grid, and the lower limit was $H=-6\pi$. The most interesting feature of Stokes waves is the concentration of total energy in the crest column with the increase of steepness. As it follows from Fig. 1 (panel 4), for Stokes waves with $AK=0.25$, a ratio of maximum value of energy $e=e_p+e_k$ to averaged energy E is about 2.5, but for Stokes waves with $AK=0.42$, this ratio is 12.6 (see last panel in Fig. 2). Such focusing of energy for critical steepness can explain the destructive power of very large steep breaking waves (freak waves).

Note that, until recently, Stokes waves were considered often as a purely mathematical object, and wave fields were investigated on a base of linear and quasilinear approaches, the surface represented as a superposition of linear waves. In reality, such surface even in animations looks unrealistic, because real waves always have sharp crests and gentle troughs. In Ref. 14, it was shown that presentation of a wave surface as a superposition of Stokes waves is considerably more compact than the traditional Fourier presentation.

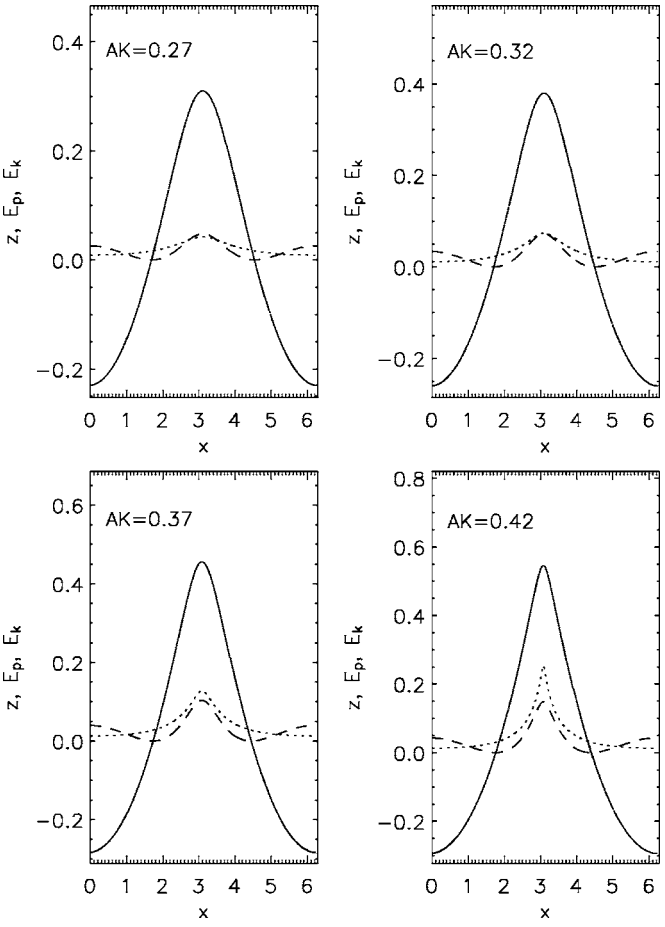

FIG. 2. Profiles of Stokes wave (solid curves), and columnar potential e_p (dashed curves) and kinetic e_k energies (dotted curves) for $AK=0.27$, 0.32, 0.37, 0.42.

IV. ADIABATIC TRANSFORMATION OF STOKES WAVES

In this study, we applied the method for the numerical simulation of surface waves developed by ChSh to investigation of the evolution of Stokes waves with the wave number K and the amplitude A (capital letters A and K are used for description of the initial conditions at $t=0$, and a,k for variables).

Choosing of the value of K is not a trivial problem. If $K=1$ is assigned, the next wave (not existing in the initial conditions) has a wave number $k=2$, so it is twice as short. Clearly, such a poor approximation imposes a restriction upon the nonlinear interactions and on the generations of the additional modes. Assigning $K=1$ is convenient for validation of the model by comparison with the analytical stationary solution, because such a "dense" presentation of waves (for example, the Stokes waves or the Crapper waves) does not leave room in the Fourier space for development of intermediate modes by instability. This is why the solution for running Stokes waves, demonstrated in Ref. 27 (and for a longer period in Ref. 14), was stable during thousands of

periods. Setting $K \geqslant 2$ (the analytical solution is described in this case by modes with the wave numbers $k=nK$, n is an integer) changes the situation dramatically: a potential possibility of development of the waves at wave numbers $[(n-1)K+1<k<(n+1)K-1]$ arises. Theoretically, these waves cannot appear in a model, but as in nature, a noise (mostly the errors of time derivatives approximation) always creates a background. It is not a matter of how small the parasitic perturbations are; they inevitably grow, resulting finally in a major transformation of the wave surface. Increasing the accuracy of the numerical scheme can delay this development, but for investigation of the geophysical fluid dynamics problems, it is not needed, because the presence of noise and development of the instability corresponds to a physical reality. Even very small-amplitude waves with $AK=0.01$ are unstable, but because the time of development of the B-F instability for small AK is proportional to $(AK)^2$, the integration should be performed for very long periods.

All calculations described below were performed initially for monochromatic waves assigned by linear theory in a range $(AK=0.05-0.40)$ with no initial disturbances. Because these waves are not a solution of steady equations, the initial wave train for $AK>0.28$ undergoes a strong modification up to clear tendency to overturning. Fast growth of modes with the wave numbers $50n$ $(n=2,3,4,\ldots)$ was observed in a very initial stage of the run. This evolution takes place at a precise conservation of the invariants: the sum of the potential and the kinetic energies preserves with an accuracy of the order of the 10^{-15} (the conservation of the horizontal momentum and volume is even better). The amplitudes on newly arisen modes are not small, and this evolution occurs for any steepness $AK \geqslant 0.05$. Strictly speaking, the pure small-amplitude monochromatic linear waves never exist. It is surprising that a new set of amplitudes was similar to a corresponding set of "bound" waves for the Stokes wave with the approximate same amplitude as the amplitude of the initial linear wave. It means that a wave crest tends to be sharper and trough to be smoother. When the initial monochromatic waves turn out into a complicated multimode wave field, the surface becomes much closer to the superposition of Stokes waves than to superposition of linear waves, as is usually assumed in quasilinear theories.[14] The same calculations performed for initially assigned exact Stokes waves showed that train of such waves is more stable. Contrary to monochromatic waves, the introducing of finite amplitude initial disturbances in this case is unavoidable. Otherwise, the growth of computational noise turns out to be very slow, which makes the approach impractical.

Finally, we choose the value $K=50$, which provides a fair approximation for growing components of the spectrum. Fourier modes for initial Stokes wave have the wave numbers $k=50n$, where $n=1,2,3,\ldots$. The individual evolutions of the wave surface for different resolutions are different, so that after disintegration of the initially homogeneous wave train, the solutions may be compared by their statistical characteristics only; for example, for the time-averaged wave spectrum. The simulations of the evolution of Stokes waves calculated by the algorithm described in Sec. II were performed for the number of modes $M=2000$, and number of grid points $N=8000$ which provided a sufficient resolution both in the Fourier and the physical spaces even for the steepest waves. An initial small-amplitude noise for variable z is assigned as a random function of number of point in grid space uniformly distributed in the range $(-10^{-6A}$ to $10^{-6}A)$. Velocity potential for noise was calculated on a base of linear theory. Time step $\Delta\tau$ was equal to 0.002. The application of a twice-shorter time step for strongly nonlinear cases proves that differences between results are negligible. Calculations were made for 42 different initial steepnesses: $AK=0.42-0.01i$, where $i=0,1,2,\ldots,41$. Stokes waves were calculated in (ξ,ζ) coordinates with the algorithm described in Sec. III, and then the solution was transferred from x coordinate to ξ coordinate. Postprocessing was done for data transferred back from (ξ,ζ) coordinates to the Cartesian coordinate by a periodic spline interpolation providing the accuracy of the order of 10^{-11} for very steep waves and 10^{-30} for small-amplitude waves. A maximum length of integration $\tau_{\max}$ was chosen equal to 4000, which corresponds to 4500 periods of the initial wave. The runs for $AK>0.13$ were terminated upon approaching to overturning. A criteria for terminating the run was defined by the first appearance of a nonsingle value of surface η:

$$x(i+1)<x(i), \quad i=1,2,3,\ldots,N-1. \tag{4.1}$$

It was possible to continue the integration after that time (see Ref. 27), but the details of this development are not a subject of this paper. It is important that after the moment when the criterion (4.1) has been reached, the solution never returns to stability: the volume of a fluid crossing the vertical $x(i)$ increases quickly. Up to this moment the conservation of the sum of the potential and the kinetic energies of the horizontal momentum and the volume was excellent. Overturning always started in a crest of the steepest wave. When a surface became a non-single value, at the initial stage of the further evolution the conservation of invariants remains good, but later, a sharp increase of energy occurs, and further integration becomes senseless. Usually it happens just for one Runge-Kutta time step, so a probable primary reason for this numerical instability is a growth of the right sides of Eqs. (2.7) and (2.8). Application of the dynamic time stepping (similar to that used in Ref. 39) can prolong this instability, but for a very short time. A primary reason of the numerical instability connected with breaking is physical: in reality the falling volume of water becomes rotational and it splits into small patterns (what appears, for example, as a whitecapping). A well-pronounced long jet simulated in Ref. 13 was probably obtained by applying a severe smoothing in a physical space. We do not apply such smoothing.

According to Benjamin and Feir instability theory[1] for first-order Stokes waves, the amplitudes of disturbances a_k in a vicinity of the main mode with the wave number $k=K$ grows exponentially:

$$a_k \propto \exp(\beta_k t), \tag{4.2}$$

In our notations, the explicit formula for β_k derived in B-F can be represented in the form

$$\beta_k = \gamma_k K^{1/2}, \quad \text{where } \gamma_k = 0.5|d_k|(2(AK)^2 - d_k^2)^{1/2}; \quad (4.3)$$

d_k characterizes the relative "distance" in a Fourier space between the modes with amplitude a_k and a main mode A_K:

$$d_k = \left[\left(\frac{k}{K}\right)^{1/2} - 1\right]. \quad (4.4)$$

Below, the function γ will be represented as a function of two parameters, i.e., AK and δ_k, where

$$\delta_k = \frac{k}{K} - 1; \quad (4.5)$$

hence,

$$d_k = (\delta_k + 1)^{1/2} - 1. \quad (4.6)$$

Numerical investigation of instability of exact Stokes waves based on linearized equation for disturbances was done in Ref. 2. It was obtained that for small d_k, the results perfectly coincide with predictions of B-F theory, but with increasing of d_k (or δ_k), the rate of growth becomes considerably less than rate predicted by B-F. It was also obtained that with increasing steepness, the one-dimensional perturbations are stable, and the most unstable become three-dimensional perturbations.

Analysis of the results of our calculations showed that the simple scenario described by Eq. (4.2) and investigated in Ref. 2 is not always complete. Fully nonlinear equations predict two regimes of development of instabilities. The examples of evolution of amplitudes for different steepness and values of d_k are given in Figs. 3 and 4. In Fig. 3 the development precisely corresponds to Eq. (4.2). After a short initial period of fast fluctuations at $t<10$, the modes $k=33$ ($d=-0.34$) (solid line) and $k=67$ ($d=0.34$) (dashed line) for steepness $AK=0.21-0.26$ grow exponentially up to reaching the quasi-equilibrium regime, when all modes fluctuate in time (see examples in Ref. 14). Newly arising modes are nearly symmetrical, relatively central modes with wave number $K=50$. The examples of the second type of evolution are represented in Fig. 4. As seen, the amplitudes of modes with wave numbers $K=10$ ($d=-0.80$) and $k=90$ ($d=0.80$) undergo two stages: slow and fast development. Obviously, B-F instability theory and numerical results[2] are valid to the first regime, and the second regime remains unexplained. The numerical model[2] assumed one-way interaction between unperturbed Stokes wave and small-amplitude disturbances. The values of β as function of AK and d_k were calculated by rms method approximating the equation

$$\log(a_k) = \log(a_0) + \beta(AK, d_k)t \quad (4.7)$$

(a_0 is an initial value of a_k) for first and second stages separately. Formal definition of point where the first regime is replaced by the second regime is difficult, and these values were chosen for each case manually. Durations of each regime (expressed in periods of Stokes wave) as a function of steepness AK are given in Fig. 5. The dotted line indicates the duration of the first stage of development.

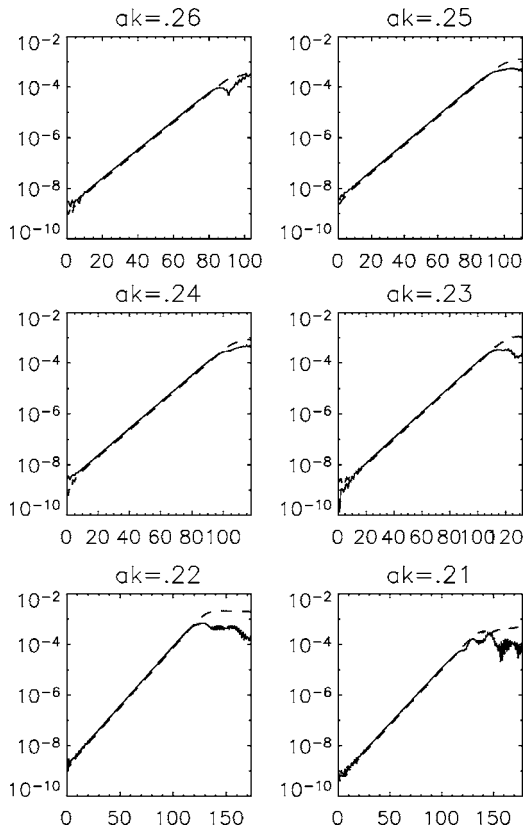

FIG. 3. Examples of first type of development: initial evolution of the amplitude of the modes with wave numbers $k=33$ ($d=-0.34$), solid line, and $k=67$ ($d=0.34$) (dashed line) for steepness $AK=0.21-0.26$. Horizontal axis corresponds to time, vertical axis to amplitude.

The time interval between dotted and dashed lines corresponds to the second period, where a growth was considerably faster than in the first period. A solid line indicates the total duration of the run up to the point of onset of breaking. For $AK=0.13$ the waves survive 1921 periods, and for $AK=0.12$, the breaking did not happen at least up to 4500 periods. Hence, critical initial steepness falls in interval [0.12, 0.13]. An attempt to define this value with a third digit was unsuccessful, because the precise evolution is sensitive to choice of initial disturbances. Generally, the data on initial development of disturbances in the first regime (curve 1) cannot be considered as absolute, because the development can be stretched by decreasing the level of the initial noise. A thick dotted line corresponds to dependence $t \propto (AK)^{-2}$ following from B-F theory. It is remarkable that this dependence is valid at least for $AK<0.15$.

An example of development of unstable modes for $AK=0.13$ is given in Fig. 6. The initial spectrum represents the modes of Stokes wave at wave numbers $k=nK$, $n=1,2,3,\ldots$ and superimposed noise. As seen, a disintegration of Stokes waves occurs in a more complicated manner than was predicted by the B-F theory: the similar disturbances grow around all modes with wave numbers $k=nK$, $n=2,3,4,\ldots$. This result confirms the prediction of

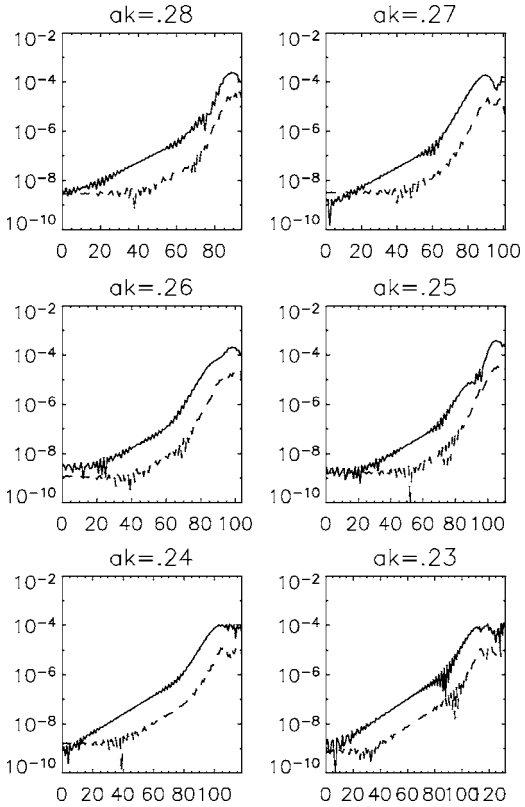

FIG. 4. The same as in Fig. 3, but for second type of development: wave numbers $k=10$ ($d=-0.80$) and $k=90$ ($d=0.80$) for steepness $AK=0.23-0.28$.

the McLean theory,[2] describing the development of one-dimensional disturbances (Class 1 in McLean's notation) in a form

$$\eta' = \sum_{-\infty}^{\infty} a_j \exp\{i[(1+\delta)jx - \sigma t]\}, \tag{4.8}$$

where a_j are the amplitudes.

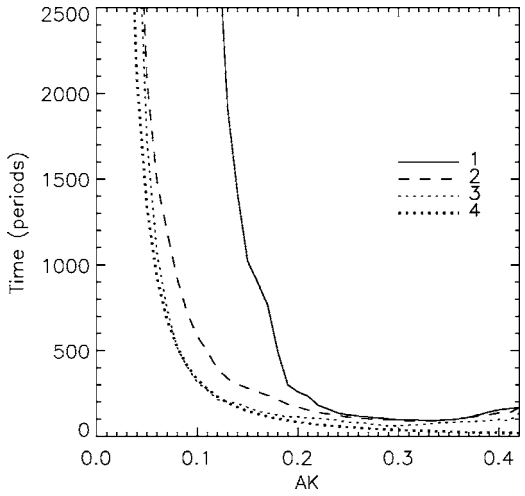

FIG. 5. Duration of the first regime (curve 3), the second regime (curve 2) and total time up to terminating of the run due to breaking onset (solid line 1) as function of initial steepness AK. Curve 4 corresponds to dependence $t \propto (AK)^{-2}$. All times are expressed in periods of a wave with wave number $K=50$.

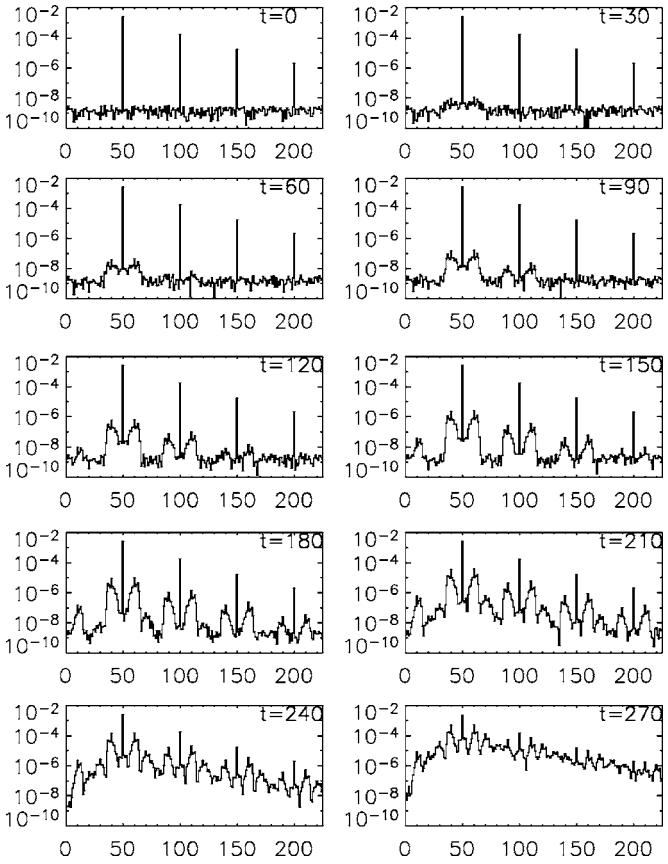

FIG. 6. Example of evolution of spectrum due to development of unstable modes for $AK=0.13$. Vertical axis corresponds to wave numbers, and horizontal axis to amplitudes.

The amplitudes of the modes arising around modes of the Stokes wave are much smaller than the amplitude of the main mode ($k=K=50$). Obviously, the bound disturbances for these modes cannot result from local interactions in the vicinity of modes with wave numbers $k=nK$ for $n>1$, because according to Eq. (4.3), the energies of these modes are too small to be able to support such a development simultaneously with developing around the first Stokes mode. Distributions of new modes growing around modes of the Stokes wave are similar to each other.

The rate of growth γ for disturbances around the first mode of the Stokes wave in the first period, as a function of δ, for different steepnesses, is shown in Fig. 7. For small steepness, the calculated data are in excellent agreement with B-F theory, but with increasing steepness, the numerical model gives smaller values of γ. The same results were obtained with linearized equations integrated in a strongly nonlinear environment (see Ref. 2). For $AK=0.40$, a linear B-F theory for a first-order Stokes wave overestimates γ by one decimal order. Numerical experiments predict also the additional areas of fast growth with the maximum on the vicinity of $\delta=\pm 0.7$. For $\delta=0.7$, this area can be referred to the area of influence of the second Stokes mode at $K=100$. These maxima are repeated around each Stokes mode. The reason for the growth of the superharmonics of the Stokes wave around $\gamma=-0.7$ is unclear. For large steepness ($AK>0.25$), the rate of growth becomes nearly constant for all δ.

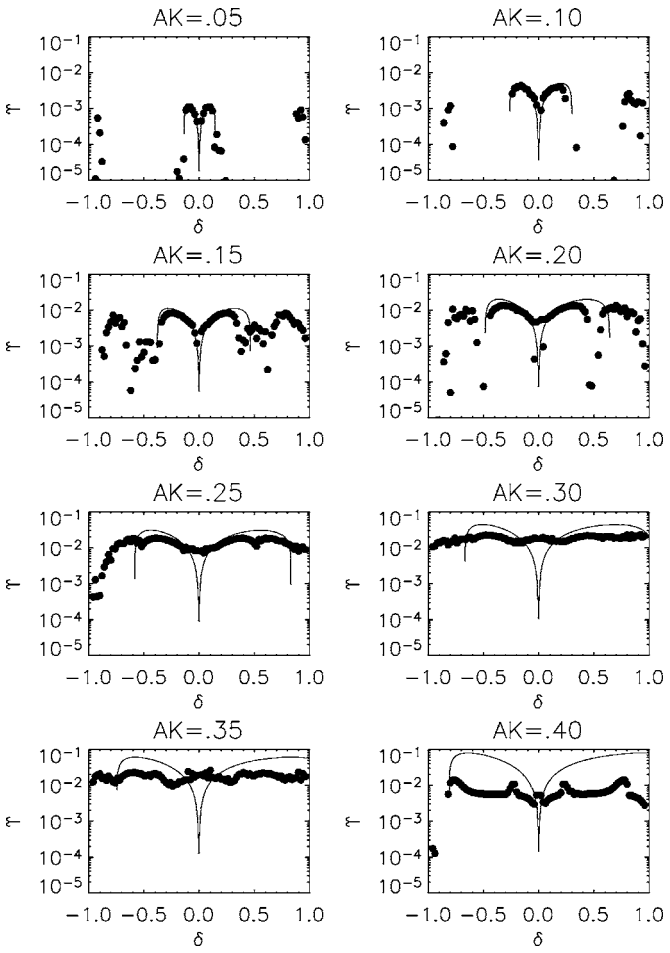

FIG. 7. Nondimensional growth rate γ in the first stage of development as function of δ and AK. Solid lines correspond to B-F analytical results; the dots are estimations obtained with Eq. (4.7).

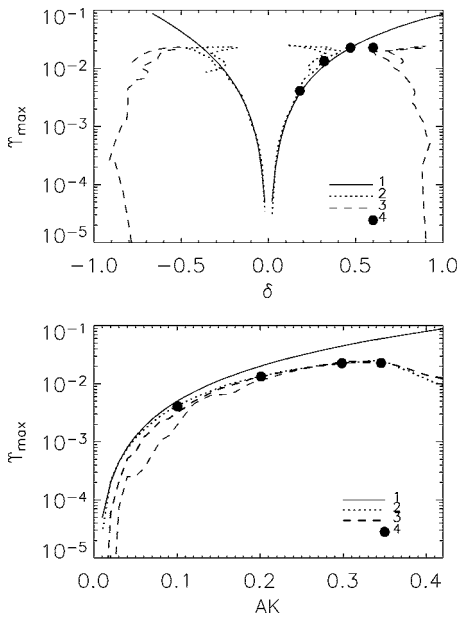

FIG. 8. Results of estimations of the growth rate for first stage. Upper panel: maximum rate of development disturbances as function of δ [Eq. (4.5)]. (1) B-F theory; (2) estimations with Eq. (4.7) for primary maximums; (3) the same estimations for secondary maximums; (4) maximum rates calculated by McLean (Ref. 2). Bottom panel: (1) B-F theory; (2) estimation with Eq. (4.7) for primary maximums (values for $\delta>0$ and $\delta<0$ practically coincide); (3) ($\delta<0$); and (4) ($\delta>0$) are estimations with Eq. (4.7) for secondary maximums.

Calculations[2] predicted a decreasing of γ at $AK>0.35$. Our calculations do not confirm this behavior, and rather support the results in Ref. 40. McLean[2] predicted the appearance of the two-dimensional disturbances for large AK, initially identified in Ref. 32. The current model, being essentially one-dimensional, predicts the unstable regime in the entire δ domain. The three-dimensional problem is to be a subject of our forthcoming paper, where a recently developed precise algorithm for three-dimensional potential waves will be described.

Data on maximum growth rate $\gamma_{\max}$ in interval $(-1<\gamma<1)$ for the first period are given in Fig. 8 (solid lines). Location of this point of relatively main mode $(\delta=0, k=50)$ is given in a top panel. As seen, for $|\delta|<0.2$, the location of maximum growth coincides precisely with predictions of B-F theory. In interval $0.2<\delta<0.4$ the results are very close to data of McLean.[2] For $\delta>0.4$, agreement with McLean calculations is poor, because locating the point of maximum is difficult (see panel for $AK=0.30$ in Fig. 7). Second maximums of growth are located around $\delta=\pm 0.8$ (dotted lines). At large AK, their positions are also unstable. The dependence of $\gamma_{\max}$ on steepness AK is given in a bottom panel (Fig. 8). Again, $\gamma_{\max}$ at small AK agrees with B-F theory, but starting from $AK=0.2$, the $\gamma_{\max}$ becomes smaller: at $AK=0.35$; it is five times smaller than in B-F theory. The same data as in Fig. 8, but for the second stage of growth, are given in Fig. 9. As seen, the rate of growth of disturbances in this stage are considerably higher than in the first stage, but for large steepnesses, the rate of growth also decreases.

The generalized data on rate of growth γ as function of steepness AK and δ for first stage are given in Fig. 10. The value $\delta=0$ corresponds to the zero mode of the Stokes wave

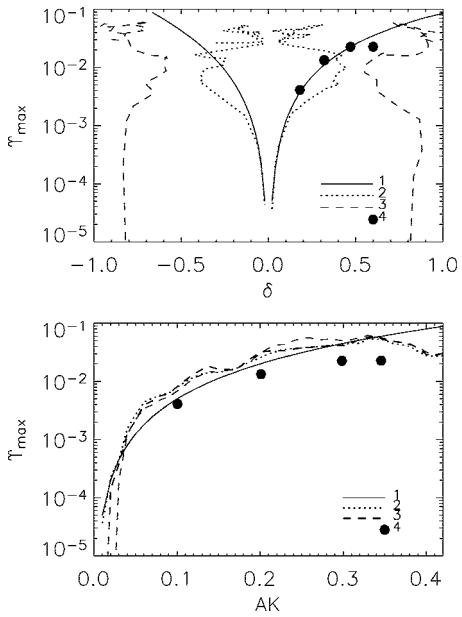

FIG. 9. The same as in Fig. 8 but for the second stage.

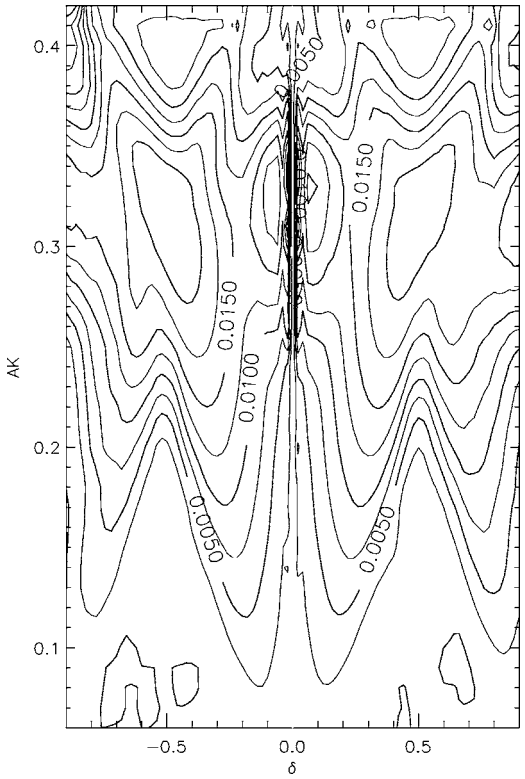

FIG. 10. Rate of growth γ (contours) in the first stage as a function of δ and AK.

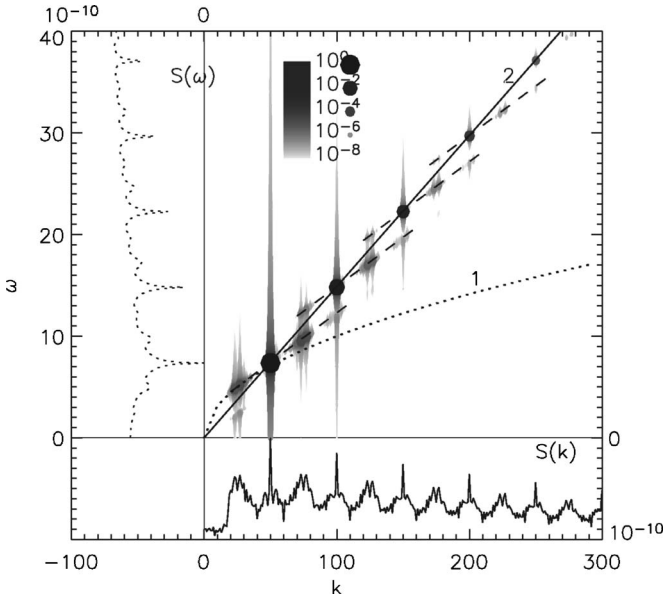

FIG. 11. Wave spectra for $AK=0.32$ obtained by averaging over the first stage of instability development. Wave-number/frequency spectrum is drawn by dots of different sizes and color (see legend and explanations in text). (1) Linear dispersive relation; (2) dispersive relations for modes of the Stokes wave. Wave-number spectrum is drawn in a bottom right quadrant (bottom horizontal axis corresponds to wave numbers, right vertical axis to wave number spectrum). Frequency spectrum is drawn in left/right quadrant (left vertical axis is a frequency, and top horizontal axis corresponds to frequency spectrum.

($K=50$). The contours of γ are nearly symmetrical with regard to $\delta=0$. The maximum value $\gamma=0.027$ was found in a point $\delta=0.5, AK=0.32$. A close value ($\gamma=0.025$) was obtained in symmetrical point $\delta=-0.5, AK=0.32$.

More specific data on disturbances in a first stage are given in Fig. 11, where the wave-number spectrum S_k, frequency spectrum S_ω, and wave-number/frequency spectrum $S_{k\omega}$ are presented. For these calculations we used the records of the amplitudes of Fourier components $\eta_k(t)$ in the Cartesian coordinate system:

$$\eta(x,t)=\sum_{-M\leqslant k\leqslant M}\eta_k(t)\vartheta_k(x), \tag{4.9}$$

where functions ϑ_k are defined by 4. Then, $\eta_k(t)$ are represented by Fourier series over time:

$$\eta(x,t)=\sum_{-M\leqslant k\leqslant M}\sum_{0<l<\Omega}h_{kl}\vartheta_l(t)\vartheta_k(x). \tag{4.10}$$

It is easy to derive that the density of spectrum $S_{k\omega}$ can be calculated by formula

$$S_{k\omega}=\tfrac{1}{2}[(h_{k,l}-h_{-k,-l})^2+(h_{k,-l}+h_{-k,l})^2], \tag{4.11}$$

and a frequency ω is connected with index l by relation

$$\omega=\frac{2\pi}{T_r}l, \tag{4.12}$$

where $T=214.26_r$ and is a length of period (consisting from 21 426 records consisting of $2M+1=4001$ Fourier amplitudes η_k through time interval $\Delta t=0.01$). Spectrum $S_{k\omega}$ is defined in a range of the wave numbers ($-M\leqslant k\leqslant M$) and in a range of the frequencies ($0\leqslant\omega\leqslant\Omega$), where Ω is a maximum frequency $\Omega=2\pi/\Delta t=200\pi$.

The solid curve in Fig. 11 corresponds to the wave-number spectrum S_k normalized to its maximum value (lower part of right axis) obtained by summation over ω:

$$S_k=\sum_{l=0,J}S_{k\omega}\Delta\omega, \tag{4.13}$$

where $J=0.5(T_r/\Delta t-1)$ is a dimension of $S_{k\omega}$ over frequencies. Dotted curves correspond to the wave-number spectrum $S_\omega(\omega)$ (left part of the top axis) normalized to its maximum value obtained by summation over k:

$$S_\omega=\sum_{k=-M,M}S_{k\omega}\Delta k. \tag{4.14}$$

Both spectra contain well-pronounced peaks at wave numbers of the Stokes wave modes. The structures of disturbances between consequent modes of Stokes wave are similar. These disturbances are pronounced less in the frequency spectrum S_ω because the amplitudes of disturbances fluctuate in time. Much more information delivers the wave-number/frequency spectrum $S_{k\omega}$. Physically, the $S_{k\omega}$ is the doubled density of the potential energy in a cell $[(k,k+\Delta k),(\omega,\omega+\Delta\omega)]$, where $\Delta k=1$ and $\Delta\omega=2\pi/T_r$. The negative values of k correspond to the waves running to opposite direction (these waves were not assigned in the boundary conditions). These waves are also generated, but their energy is small, and we will not consider them. Actually, the spectrum $S_{k\omega}$ decreases quickly with the growth of k and ω, so that we represent a domain only for relatively low wave, positive

wave numbers ($k<300$) and low frequencies ($\omega<40$). The spectra $S_{k\omega}$ are represented in Fig. 10 for the initial stage of the run with $AK=0.32$. The left axis corresponds to the frequency ω, the bottom axis to the wave number k. The spectrum is drawn by circles with different colors, for which size and blackness depend linearly on $\log_{10}(S_{k\omega})$ (see legend). Hence, the main components of the Stokes waves correspond to black circles, and small disturbances to gray dots. All components of Stokes wave lie precisely on a straight line (2) corresponding with accuracy up to four digits to theoretical seventh-order phase velocity of Stokes waves $C_s=0.1488$. The dotted line represents a dependence $\omega=k^{1/2}$ (linear phase velocity for $k=50$ equals to 0.1414). The disturbance are represented by their averaged values for the entire first stage of development, so that their actual values to the end of this period are larger than those represented in Fig. 11. The amplitudes of modes of Stokes wave in a presence of disturbances are not the constants, due to fast (and obviously reversible) nonlinear interaction between modes and disturbances. This is why each point corresponding to Stokes wave modes is surrounded by a broad vertical halo (gray vertical lines, aggregated, in fact, from a large number of gray points). The additional modes (growing due to B-F instability between Stokes wave modes), also have variable amplitudes. Each mode of the Stokes wave is surrounded by two families of disturbances arising below and above the wave number of mode k_s of the Stokes wave. The disturbances with $k<k_s$ move faster than the Stokes wave, and the disturbances at $k>k_s$ moves more slowly. Only the first group of waves, which are superharmonics for the Stokes wave, satisfy well the linear dispersive relation. All other growing modes cannot be attributed to free waves (because they lie far away from the dotted line corresponding to linear dispersive relation) and neither to bound waves of Stokes waves (because they do not fall on a solid straight line). The connection between frequency ω and wave number k for disturbances may be approximated by formula

$$\omega=\omega_s+c_k(k-k_s), \tag{4.15}$$

where $\omega_s=C_sk_s$ are frequencies of Stokes modes. Dependences (4.15) are shown in Fig. 11 by dashed lines. Remarkably, those disturbances grow symmetrically relative to Stokes modes in wave-number space, and empirical coefficient $c_k=0.097$ preserves its value with good accuracy for all Stokes modes.

V. QUASISTATIONARY REGIME

Time of development of the instability (see Fig. 5) depends strongly on initial nonlinearity, characterized by steepness AK. The evolution of 25 modes with wave numbers $k=25+2n$, $n=1,2,3,\ldots,25$ for $AK=0.15$ is shown in Fig. 12. It is seen that some modes are developing exponentially up to reaching quasistationary regime, and other modes are developing in two stages: slow and fast. To the end of this development the disturbances take most part of energy of zero Stokes mode. Finally, wave surface becomes a random superposition of running nonlinear waves with fluctuating amplitudes. This quasistationary regime was explicitly simulated for all steepness $AK\geqslant 0.04$. Presumably, for smaller steepness, this regime can be reached as well, but the time scale for development of the B-F instability increases as $(AK)^{-2}$ (see Fig. 5, curve 4); hence, such development takes a very long time. The final surface on the way to breaking (bottom panel in Fig. 13) is a typical multimode wave surface. Note that the peak of spectrum in a quasistationary regime shifted to lower wave numbers compared with its initial location.

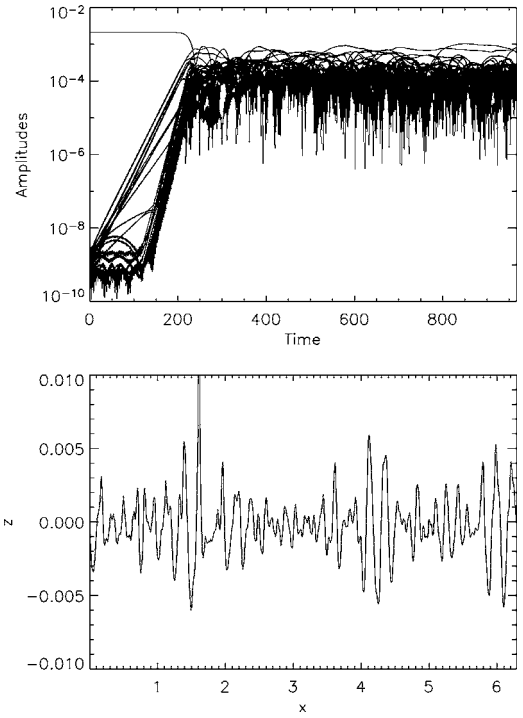

FIG. 12. Top panel: evolution of amplitudes of modes with wave numbers $k=25+2n$, $n=1,2,3,\ldots,25$ adjacent to the main mode of the Stokes wave ($K=50$). Bottom panel: last recorded surface z before breaking.

The nature of the modes arising due to nonlinearity is fairly complicated. Simulated quasistationary regime for $t>250$ was used for calculations of phase velocities and spectrum (top and bottom panels in Fig. 13). A calculation of an instantaneous value of the phase velocity of the kth wave component can be done with the relation

$$c_k=\frac{z_{-k}\dfrac{\partial z_k}{\partial\tau}-z_k\dfrac{\partial z_{-k}}{\partial\tau}}{k(z_k^2+z_{-k}^2)}, \tag{5.1}$$

where the derivatives on time are calculated for z transferred to Cartesian coordinates. For increasing accuracy, Eq. (5.1) was used for the rms method:

$$\overline{c_k}=\frac{\overline{CD}}{\overline{D^2}}, \tag{5.2}$$

where $\overline{c_k}$ is a mean phase velocity, C is the numerator, and D is the denominator in (5.1).

For developed spectrum, the lowest modes ($k=20-80$) obey the dispersive relation, but phase velocities for high wave numbers are larger than phase velocity for linear waves. A simple explanation for these phenomena was given

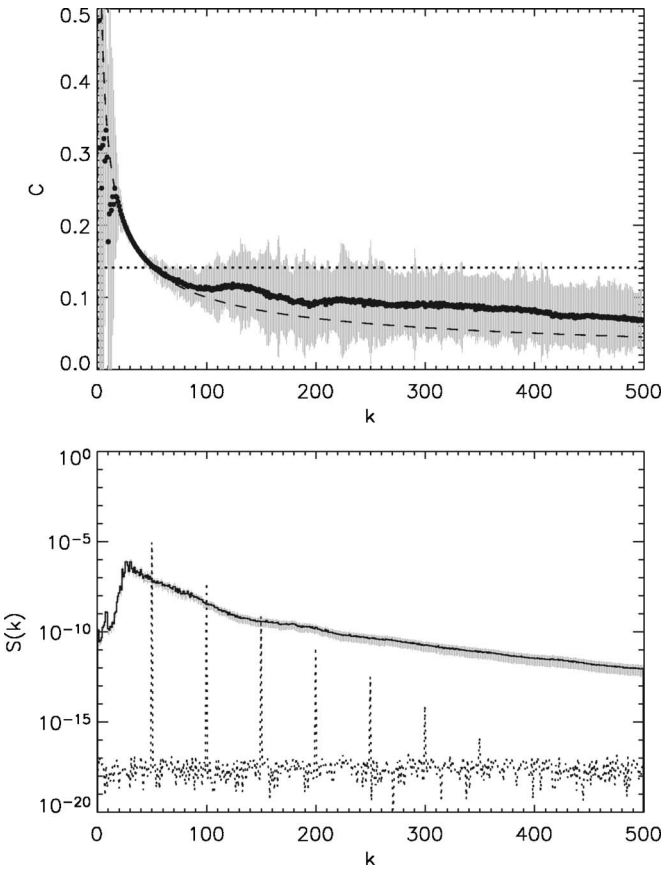

FIG. 13. Characteristics of wave field in quasistationary regime for $AK=0.15$, $250<t<950$. Top panel: phase velocity c as function of wave number k calculated with Eq. (5.2). Dotted line corresponds to initial phase velocity of Stokes wave, $c_s=0.1488$ dashed lane is a linear dispersive relation $c=k^{1/2}$. Bottom panel: wave spectrum in quasistationary regime. Gray vertical lines characterize the scatter of spectrum; gray dotted line corresponds to initial spectrum of Stokes wave.

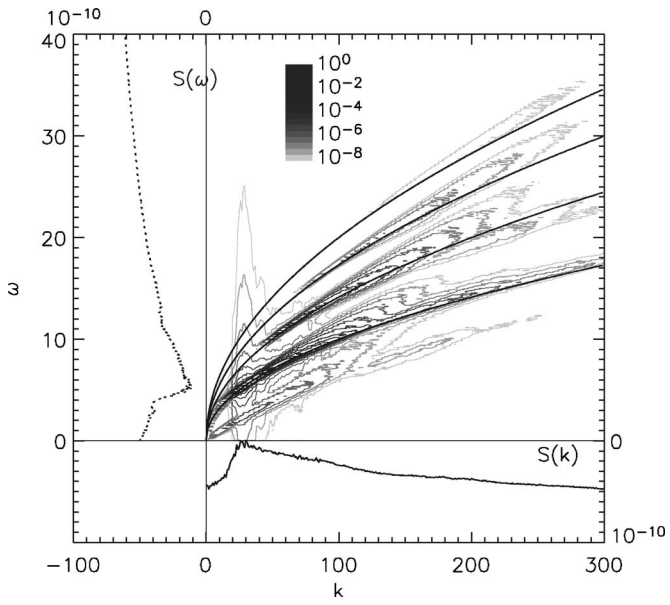

FIG. 14. The same as in Fig. 11, but for $AK=0.15$, $250<t<950$. Solid lines correspond to generalized dispersive relation [Eq. (5.5)] for $n=0,1,2,3$.

by ChSh. In fact, at each wave number several modes coexist: one is a free wave; all others are so-called bound waves corresponding to the additional modes attached for every steep enough wave. Naturally, these bound waves run with the phase velocity of the carrying wave. The calculations of phase velocity based on (5.2) give a weighted value between the velocities of free and several bound modes. Evidently, the nonlinear waves cannot obey a strict dispersion relation $\omega=k^{1/2}$ because calculation type of relation (5.1) assumes that amplitude of any wave $A_k=(a_k^2+a_{-k}^2)^{1/2}$ remains constant. Figure 12 and statistical data on "lifetime" of waves given in Fig. 5 by Chalikov[14] testify that only low-wave-number modes with large amplitudes remain more or less steady. For high-wave-number modes, a time scale of unsteadiness is the order of one period; these waves are rather a nonlinear object, than free waves. Scatter of dispersion relation may be also increased by Doppler effects: phase velocity of short waves is affected by orbital velocity fields, produced by all waves.

The formation of additional branches of the spectrum may be easily explained. Let us suppose that the wave field represented by a set of nonlinear waves, and the frequencies of main modes ω_{i0} satisfies the dispersive relation

$$\omega_{i0}=k_i^{1/2}[1+f(a_ik_i)]^{1/2}, \tag{5.3}$$

where f is a function correcting the linear dispersive relation for the case of finite amplitude. Let us define that (5.3) corresponds to bound mode of zeroth order and find a frequency of nth-order bound mode ω_{kn} $(n=1,2,3,\ldots)$ at wave number k. The bound mode has the same phase velocity as its carrying main mode with the wave number $k_m=k/(n+1)$ and frequency $\omega_m=k_m^{1/2}$. Hence, a frequency of nth-order bound mode ω_{kn} can be found from the proportion

$$\frac{k_m}{\omega_m}=\frac{k}{\omega_{kn}}, \tag{5.4}$$

and general dispersion relation for any order of bound modes obtains the form

$$\omega_{kn}=[(n+1)k]^{1/2}[1+f(a_mk_m)]^{1/2}, \tag{5.5}$$

where $k_m=k/(n+1)$ and $\omega_m=k_m^{1/2}$ are the wave number and frequency of the carrying wave, respectively. Neglecting the correction f, Eq. (3.6) obtains a simple form:

$$\omega_{kn}=[(n+1)k]^{1/2} \tag{5.6}$$

the branches for $n=0,1,2$ $(k>0)$ and $n=0$ $(k<0)$ are drawn in Fig. 14 by thin lines. Three branches of dispersive relation (5.6) for $n=0,1,2(k>0)$, for $n=0(k<0)$ and are clearly pronounced. However, the spectrum reveals many new features, an explanation of which is not easy. First, all dependencies of frequency on wave numbers have large scatter, increasing with the growth of wave numbers. Second, for all branches, the dependence of the frequencies on wave numbers systematically declines for dispersion relation (5.6) at high wave numbers. Probably, this effect can be explained by the high nonsteadiness of these modes. Third, there is a linear branch $\omega=0.14k$, which probably reflects the group effects. A contribution of different branches into total energy is represented in Fig. 10, where the $S_{k\omega}$ is represented as a function of

frequency ω for different (only positive) wave numbers $k=25n$, $n=1-8$. Note that the results represented in Fig. 9 (bottom panel) are similar to results obtained by Chalikov and Sheinin (Ref. 27, Fig. 10), where up to 14 branches of dispersion relation were found.

Note that calculations of a well-defined wave number-frequency spectrum even for 1-D waves need a very long time series. For calculation of spectrum in one panel in Fig. 9, a number of "measurements" as large as 2.4×10^8 were used. These data can be considered as "precise." Analogous calculations with observational data need a much larger volume of data, which is why just plain confirmations of linearity usually have been obtained.

A clearly pronounced positive skewness of the nonlinear waves (see Ref. 14) makes it reasonable to suppose that a superposition of the Stokes waves could be better model of gravity waves surface than a superposition of the linear waves. Let us consider the maximum error $e^l_{\max}(m)$ of approximation the wave profile by the Fourier series in Cartesian coordinates [linear presentation, compare with Eq. (2.3)]:

$$e^l_{\max}=\overline{\max\left(\left|\sum_{k=-m}^{k=m} h_k\vartheta_k(x)-\eta(x)\right|\right)},\qquad m=1,2,3,\ldots,M, \tag{5.7}$$

where an extreme is found over period $(0,2\pi)$ for each of the recorded wave profiles. Then, $e_{\max}(m)$ was averaged over the entire ensemble of recorded wave profiles in quasistationary regime (after the initial trail of Stokes waves has been completely destroyed). Evidently, e_m is a monotonic decaying function of m. We can also calculate the error of approximation of the wave surface by the partial sums of the Stokes modes $\sigma_k S(k,\sigma_k,\varphi_k)$ (σ_k are the amplitudes and φ_k are the phases of the Stokes waves with a wave number k):

$$e^s_{\max}=\overline{\max\left(\left|\sum_{k=-m}^{k=m} \sigma_k S(k,\sigma_k,\varphi_k)-\eta(x)\right|\right)}. \tag{5.8}$$

Because the shape of the Stokes wave S_k depends on its amplitude σ_k, and analytical presentation S_k is unavailable, a calculation of (5.8) represents a nonlinear minimization problem: complicated but still resolvable. Such minimization may be done with a precalculated large set of Stokes waves by an algorithm described by ChSh. Unexpectedly, a very simple solution of this problem was found when a coupled water/air problem was considered (see Refs. 5 and 11). The equations for a boundary layer above waves were formulated in conformal coordinates analogous to (2.1) and (2.2), but for upper domain $z>\eta$. The upper system of coordinates (ξ_u,ζ_u) has an opposite "density" compared with the lower coordinates: where Jacobian on a surface in lower coordinates it is large, in upper coordinates it is small. The Stokes wave (calculated by the algorithm described by ChSh), being transferred to upper coordinate, turned out to be there with a high accuracy a single Fourier mode $a_k\vartheta_k(\xi_u)$. Thus, the surface $\eta(\xi_u)$ may be presented as a superposition of elementary Fourier modes $a_k\vartheta_k(\xi_u)$ in the upper coordinates. The function $\eta(\xi_u)$ was transferred to $\eta(x)$ by periodic spline interpolation.

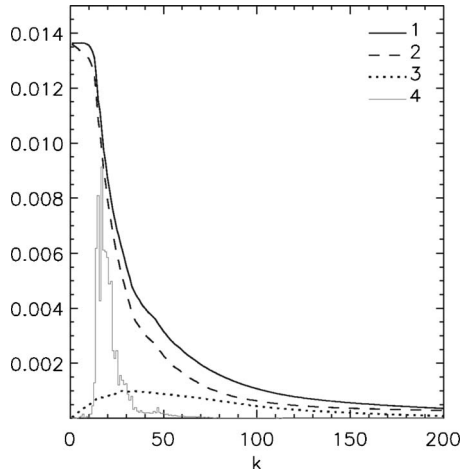

FIG. 15. Dependences of the errors of approximations on truncation wave number m: (1) error of approximation $e^l_{\max}$; (2) $e^s_{\max}$; (3) their difference $e^l_{\max}-e^s_{\max}$; (4) averaged wave spectrum $5000S_k$.

The errors of approximation of the wave surface by linear waves (solid line) and by Stokes waves (dashed line) are represented in Fig. 15. The differences between these two types of errors $e^l_{\max}-e^s_{\max}$ are given by a dotted line. Evidently, the set of Stokes waves approximates a surface much better than the same number of linear waves. In all cases, the maximum difference is located in the wave crests. Thus, for many practical applications (remote sensing, wind-wave interaction), a superposition of Stokes waves with random phases is better than traditional linear presentation.

VI. DISCUSSION AND CONCLUSIONS

In this study, we applied the method for numerical simulation of periodic surface waves, developed by ChSh, to a long-range simulation of initially homogeneous Stokes wave train contaminated with a small initial noise. The initial condition representing the exact Stokes waves with steepness $AK=0.01-0.42$ are calculated with a simple and very fast algorithm developed for stationary solution. It is shown that high amplitude Stokes waves are characterized by sharp focusing of energy around wave peak (see Figs. 1 and 2). This effect can explain the nature of freak waves. The principal nonstationary equations are the standard equations of hydrodynamics for potential flow with a free surface. The numerical method is based on a nonstationary conformal transformation that maps the original domain (which may be of finite or infinite depth) onto a domain with a fixed rectilinear upper boundary. It is shown that initial development of disturbances agrees with B-F instability theory up to steepness $AK=0.1$, and for larger steepness with the results of Ref. 2. The unstable modes develop around each mode of Stokes waves, as was predicted in Ref. 2. In most cases, the initial relatively slow growth is followed by the second stage of development (Fig. 4), when growth occurs several times faster than in a first stage. A development in a second stage is characterized by decreasing of energy of zero mode; hence, it

occurs under the control of conservations laws. The dependence of the rate of growth γ in the first stage is calculated in a broad range of wave numbers and steepnesses (see Fig. 10). The calculated wave-number/frequency spectrum shows that newly arising waves cannot be referred to as free linear waves or as bound waves of Stokes waves. All Stokes waves (at least with $AK \geqslant 0.04$) finally disintegrate and create quasistationary multimode regime (Fig. 12). For steepness $AK > 0.12$ one of the waves comes to overturning, terminating the run. Wave fields created by Stokes waves with initial steepness $AK \leqslant 0.12$ are virtually stable. A threshold $0.12 < (AK)_c < 0.13$ is established accurately. It does not depend on resolution of model and wave number of zero mode of Stokes wave. A definition of more precise value of $(AK)_c$ is difficult because the development depends on structure and amplitudes of initial noise. Phase velocities of low wave number waves at $K < 20$ are difficult to calculate because of their low energy. In the energy-containing part of spectrum $(20 < k < 60)$, waves in quasistationary regime agree strictly with linear theory, but for larger wave numbers, phase velocity is systematically higher than phase velocity of linear waves. This happens because the calculations of phase velocity based on (5.2) give a weighted by energy value between the velocities of free and several bound modes. Calculations of the wave-number/frequency spectrum prove that dispersive relation consists of several branches. Each of them corresponds to a different order of bound waves. An explicit form of dispersive relation has been derived. The wave surface can be represented by the set of Stokes waves much more accurately than by superposition of the linear modes.

The applicability of the 1-D approach and potential assumption to high frequency waves is questionable. This approach obviously cannot properly simulate the processes where irreversible 2-D nonlinear interactions are of the essence. Of course, all nonlinear effects in the 2-D case should be more clearly pronounced because of an infinitely larger number of interacting modes and physically because of a complexity of the orbital velocity field. The model developed may be applied to a broad range of situations in which the 1-D approximation is acceptable. Fortunately, many wave phenomena are largely controlled by strong nonlinear interactions which are relatively fast and for which the 1-D approximation is often adequate. Formation of extreme waves is one such phenomenon. As yet, model simulations of very large waves are far from merely academic interest. It has long been known that nonlinear redistribution of energy can result in the abrupt emergence of very large and steep waves, commonly known as *freak* or *rogue* waves.

The most important application of the scheme developed here is the *coupled modeling* of waves and wave boundary layer (see Ref. 11), which has been completed and it will be a subject of our next publications. For these purposes the 1-D wave model is acceptable because it reproduces a broad spectrum of waves and surface disturbances having realistic shapes; these, in turn, generate rich statistics of nonlinear fluctuations in an air flow above waves. It was always desirable but never proved that the multimode wave surface interacts with the atmosphere as a set of independent linear waves, and that the integral result can be obtained by simple superposition of the monochromatic cases. It is well known that even a single wave can produce a broad spectrum of pressure fluctuations that affect the flow. Atmospheric response to a strongly nonstationary wave field is also essentially nonstationary. The structure of nonstationary flow (e.g., a distribution of surface pressure) is always different than that of stationary. A proper way to investigate the wind-wave interaction problem is a long-term integration of a coupled system (including the model discussed above) and appropriate processing of the results. Surely, the spectral considerations are unavoidable, because they have important practical application (for source terms for wind waves forecasting models). However, the most complicated and transient processes (breaking wave, freak waves, flow separation with and without breaking) occur in a physical space. These processes deserve special attention.

Surely, a one-dimensional approach to modeling of sea waves is incomplete, because of weaker nonlinearity compared with two-dimensional cases. At present, the precise three-dimensional (3-D) model based on principal potential equations has also been completed. Being applied to 1-D waves, performance of this model is just slightly less than performance of the 1-D model based on conformal mapping. However, in view of a much larger number of degrees of freedom in 3-D cases, simulation of such waves represents a formidable computational problem. Fortunately, this model can be effectively parallelized.

ACKNOWLEDGMENTS

The authors wish to thank unknown reviewers for their valuable comments and suggestions as well as Sandra Stitt, who edited the manuscript making a number of improvements.

[1] T. B. Benjamin and J. E. Feir, "The disintegration of wave trains in deep water," J. Fluid Mech. **27**, 417 (1967).
[2] J. W. McLean, "Instabilities of finite-amplitude water waves," J. Fluid Mech. **114**, 315 (1982).
[3] P. R. Gent and P. A. Taylor, "A numerical model of the air flow above water waves," J. Fluid Mech. **77**, 105 (1976).
[4] D. Chalikov, "The numerical simulation of wind-wave interaction," J. Fluid Mech. **87**, 561 (1978).
[5] D. V. Chalikov, "Numerical simulation of the boundary layer above waves," Boundary-Layer Meteorol. **34**, 63 (1986).
[6] V. K. Makin, "A note on wind speed and sea state dependence of the heat exchange coefficient," Boundary-Layer Meteorol. **91**, 127 (1999).
[7] C. Mastenbroek, V. K. Makin, M. H. Garat, and J. P. Giovanangeli, "Experimental evidence of the rapid distortion of the turbulence in the air flow over water waves," J. Fluid Mech. **318**, 273 (1996).
[8] J. F. Meirink and V. K. Makin, "Modeling low-Reynolds-number effects in the turbulent air flow over water waves," J. Fluid Mech. **415**, 155 (2000).
[9] P. Y. Li and P. A. Taylor, "Second order turbulence closure modeling for air flow over water waves," Boundary-Layer Meteorol. **95**, 397 (2000).
[10] M. L. Banner, "The influence of wave breaking on the surface pressure distribution in wind-wave interaction," J. Fluid Mech. **211**, 463 (1990).
[11] D. Chalikov, "Interactive modeling of surface waves and boundary layer," in *Ocean Wave Measurements and Analysis: Proceedings of the Third International Symposium on Waves 97* (American Society of Civil Engineers, Reston, VA, 1998), pp. 1525–1540.
[12] J. W. Dold and D. H. Peregrine, "An efficient boundary-integral method for steep unsteady water waves," in *Numerical Methods for Fluid Dynamics*, edited by K. W. Morton and M. J. Baines (Oxford University Press, New York, 1986).

[13] J. W. Dold, "An efficient surface-integral algorithm applied to unsteady gravity waves," J. Comput. Phys. **103**, 90 (1992).
[14] D. Chalikov, "Statistical properties of nonlinear one-dimensional wave fields," Nonlinear Processes Geophys. **12**, 671 (2005).
[15] W. T. Tsai and D. K. P. Yue, "Computation of nonlinear free-surface flows," Annu. Rev. Fluid Mech. **28**, 249 (1996).
[16] K. L. Henderson, D. H. Peregrine, and J. W. Dold, "Unsteady water wave modulations: fully nonlinear solutions and comparison with the nonlinear Schrodinger equation," Wave Motion **29**, 341 (1999).
[17] G. D. Crapper, "An exact solution for progressive capillary waves of arbitrary amplitude," J. Fluid Mech. **96**, 417 (1957).
[18] G. D. Crapper, *Introduction to Water Waves* (John Wiley, Chichester, 1984), p. 224.
[19] G. G. Stokes, "On the theory of oscillatory waves," Trans. Cambridge Philos. Soc. **8**, 441 (1847); *Mathematical and Physical Papers* (Cambridge University Press, Cambridge, 1847), Vol. 1, p. 197.
[20] G. G. Stokes, "Supplement to a paper on the theory of oscillatory waves," in *Mathematical and Physical Papers* (Cambridge University Press, Cambridge, 1880), Vol. 1, pp. 314–326.
[21] J. V. Whitney, "The numerical solution of unsteady free-surface flows by conformal mapping," in *Proceedings. Second International Conference on Numerical Fluid Dynamics*, edited by M. Holt (Springer-Verlag, Berlin, 1971), pp. 458–462.
[22] T. Kano and T. Nishida, "Sur le ondes de surface de l'eau avec une justification mathematique des equations des ondes en eau peu profonde," J. Math. Kyoto Univ. **19**, 335 (1979).
[23] B. Fornberg, "A numerical method for conformal mapping," SIAM (Soc. Ind. Appl. Math.) J. Sci. Stat. Comput. **1**, 386 (1980).
[24] D. I. Meiron, S. A. Orszag, and M. Israeli, "Applications of numerical conformal mapping," J. Comput. Phys. **40**, 345 (1981).
[25] S. Tanveer, "Singularities in water waves and Rayleigh-Taylor instability," Proc. R. Soc. London, Ser. A **435**, 137, (1991).
[26] S. Tanveer, "Singularities in the classical Rayleigh-Taylor flow: Formation and subsequent motion," Proc. R. Soc. London, Ser. A **441**, 501 (1993).
[27] D. Chalikov and D. Sheinin, "Direct modeling of one-dimensional nonlinear potential waves," in *Nonlinear Ocean Waves*, Advances in Fluid Mechanics Vol. 17, edited by W. Perrie (WIT Press, Southampton, UK, 1998), pp. 207–258.
[28] A. I. Dyachenko, E. A. Kuznetsov, M. D. Spector, and C. E. Zakharov, "Analytical description of the free surface dynamics of an ideal fluid (canonical formalism and conformal mapping)," Phys. Lett. A **221**, 73 (1996).
[29] R. Menikoff and C. Zemach, "Methods for numerical conformal mapping," J. Comput. Phys. **36**, 366 (1980).
[30] D. Chalikov and D. Sheinin, "Modeling of extreme waves based on equations of potential flow with a free surface," J. Comput. Phys. **210**, 247 (2005).
[31] M. J. Lighthill, "Contribution to the theory of waves of finite amplitude in nonlinear dispersive system," IMA J. Appl. Math. **1**, 269 (1965).
[32] M. C. Longuet-Higgins" The instabilities of gravity waves of finite amplitude in deep water. II: Suharmonics," Proc. R. Soc. London, Ser. A **360**, 489 (1978).
[33] W. K. Melville, "The instability and breaking of deep-water waves," J. Fluid Mech. **115**, 165 (1982).
[34] P. G. Schwartz, "Computer extension and analytic continuation of Stokes expansion for gravity waves," J. Fluid Mech. **62**, 553 (1974).
[35] P. G. Saffman, "Long wavelength bifurcation of gravity waves on deep water," J. Fluid Mech. **101**, 567 (1980).
[36] J. D. Fenton, "The numerical solution of steady water wave problems," Comput. Geosci. **14**, 357 (1988).
[37] W. M. Drennan, W. N. Hui, and G. Tenti, "Accurate calculations of Stokes water waves of large amplitude," ZAMP **43**, 367 (1992).
[38] D. Sheinin and D. Chalikov, "Hydrodynamical modeling of potential surface waves," in *Problems of Hydrometeorology and Environment on the Eve of XXI Century, Proceedings of International Theoretical Conference, St. Petersburg*, 24–25 June 1999 (Hydrometeoizdat, St.-Petersburg, 2000), pp. 305–337.
[39] V. E. Zakharov, A. I. Dyachenko, and O. A. Vasilyev, "New method for numerical simulation of a nonstationary potential flow of incompressible fluid with a free surface," Eur. J. Mech. B/Fluids **21**, 283 (2002).
[40] C. Kharif and A. Ramamonjiarisoa, "On the stability of gravity waves on deep water." Phys. Fluids **31**, 1286 (1988).